

Upgrade of NaI(Tl) crystal encapsulation for the NEON experiment

J. J. Choi,¹ E. J. Jeon,^{2,3} J. Y. Kim,⁴ K. W. Kim,² S. H. Kim,² S. K. Kim,¹ Y. D. Kim,^{2,3} Y. J. Ko,² B. C. Koh,⁵ C. Ha,⁵ B. J. Park,² S. H. Lee,^{3,2} I. S. Lee,² H. Lee,^{3,2} H. S. Lee,^{2,3} J. Lee,² and Y. M. Oh²

((NEON Collaboration))

¹*Department of Physics and Astronomy, Seoul National University, Seoul 08826, Republic of Korea*

²*Center for Underground Physics, Institute for Basic Science (IBS), Daejeon 34126, Republic of Korea*

³*IBS School, University of Science and Technology (UST), Daejeon 34113, Republic of Korea*

⁴*Korea Atomic Energy Research Institute, Daejeon 34057, Republic of Korea*

⁵*Department of Physics, Chung-Ang University, Seoul 06973, Republic of Korea*

The Neutrino Elastic-scattering Observation with NaI(Tl) experiment (NEON) aims to detect coherent elastic neutrino-nucleus scattering ($\text{CE}\nu\text{NS}$) in a NaI(Tl) crystal using reactor anti-electron neutrinos at the Hanbit nuclear power plant complex. A total of 13.3 kg of NaI(Tl) crystals were initially installed in December 2020 at the tendon gallery, 23.7 ± 0.3 m away from the reactor core, which operates at a thermal power of 2.8 GW. Initial engineering operation was performed from May 2021 to March 2022 and observed unexpected photomultiplier-induced noise and a decreased light yield that were induced by leakage of liquid scintillator into the detector due to weakness of detector encapsulation. We upgraded the detector encapsulation design to prevent leakage of the liquid scintillator. Meanwhile two small size detectors were replaced with large size detectors returning a total mass of 16.7 kg. With this new design implementation, the detector system has been operating stably since April 2022 for over a year without detector gain drop. In this paper, we present an improved crystal encapsulation design and stability of the NEON experiment.

INTRODUCTION

The coherent elastic neutrino-nucleus scattering ($\text{CE}\nu\text{NS}$) is a process predicted by the Standard Model [1, 2]. Due to its potential role in enhancing the standard model comprehension [3–5] and exploring new physics phenomena [6–8], $\text{CE}\nu\text{NS}$ has garnered the interest of particle physicists. Numerous experiments aiming to detect $\text{CE}\nu\text{NS}$ and employing advanced detector technologies were proposed, with some being successfully executed [9–19]. However, they encountered challenges arising from the minuscule deposited energy (on the order of keV) into the nucleus.

The COHERENT collaboration reported the detection of $\text{CE}\nu\text{NS}$ using a conventional CsI(Na) detector with a stopped-pion source from the SNS accelerator in 2017 [20]. Following this, the same research team verified the process using a liquid argon detector [21]. The resulting signal includes, in part, the incoherent scattering at the neutrino energy of ~ 30 MeV [15]. Therefore, the investigation of $\text{CE}\nu\text{NS}$ in the fully coherent regime using the few MeV antineutrinos from a nuclear reactor can provide precise information for understanding neutrinos. This represents a crucial avenue for exploring non-standard neutrino interactions [10, 22–24], modeling supernova energy transport in astrophysics [25], and monitoring nuclear reactors [26, 27].

In particular, reactor neutrinos with energies reaching a few MeV produce visible recoils with energy less than 1 keV, significantly lower than the typical energy threshold of a kg-size particle detector. Extensive scientific efforts are focused on the search for $\text{CE}\nu\text{NS}$ in close proximity to commercial power or experimental nuclear

reactors. Different experimental techniques are used to detect and investigate $\text{CE}\nu\text{NS}$. Several experiments are currently running or under construction: CONUS [19], COHERENT [28], NUCLEUS [18], CONNIE [14], and νGeN [12].

Neutrino elastic scattering observation with NaI (NEON) is an experiment that aims to observe $\text{CE}\nu\text{NS}$ using reactor antineutrinos from reactor unit 6 at the Hanbit nuclear power plant complex. Utilizing the expertise of NEOS, a short baseline reactor neutrino experiment [29], and the experience of developing a high light yield NaI(Tl) detector in the COSINE-100 experiment, a dark matter search experiment [30, 31], the NEON experiment progressed smoothly from the initial development to the installation of the reactor site in December 2020. NaI(Tl) crystals for NEON detector are applied a novel technique of crystal encapsulation that significantly increased the light collection efficiency and obtained approximately 22 number of photoelectrons (PEs) per unit keV electron-equivalent energy (keVee) [32, 33], which was approximately 50% larger than the light yield of COSINE-100 crystals [34]. The six NaI(Tl) crystal detector are immersed in 800 L of liquid scintillator (LS) for active reduction of radioactive backgrounds [35]. The LS is surrounded by 10 cm lead, 2.5 cm borated-polyethylene, and 20 cm polyethylene to reduce the background contribution from external radiation [33]. To monitor the initial performance and detector stability, the engineering operation was performed from May 2021 to Mar 2022 using 13.3 kg NaI(Tl) crystals at full reactor unit operational power. During the engineering-run, we found that the crystal light yield gradually decreased and unexpected photomultiplier (PMT)-induced noise caused

by leakage of LS into the detector due to weakness of detector encapsulation. Thus we upgraded crystal encapsulation design to reject PMT-induced noise and improve gain stability performance. In addition, two small-size crystals, which had relatively smaller light yield and higher backgrounds that were NEO-1 and NEON-2 in Ref. [33], were replaced with large-size crystals and the total mass of the NEON experiment increased to 16.7 kg. Under these upgraded conditions, physics-run have been operating smoothly since April 2022. In this paper, we describe the new encapsulation design of the NaI(Tl) crystals and the stable operational status following the encapsulation upgrade of the NEON experiment.

NEON ENCAPSULATION DESIGN

The NEON experiment utilized six commercial-grade NaI(Tl) crystals manufactured by Alpha Spectra Inc. (AS). In engineering run, a total of 13.3 kg of NaI crystals were employed: four with a 3-inch diameter and 4-inch length, and two with a 3-inch diameter and 8-inch length. To maximize the measured light yields while safeguarding NaI(Tl) from moisture due to its hygroscopic property, we applied a novel technique for crystal encapsulation to NEON detectors [32]. This design minimizes the optical interface between the crystal and PMT by utilizing an optical pad (silicon rubber EJ-560 from Eljen technology) to efficiently collect scintillation photons. Crystals and PMTs are encapsulated within a copper case, exposing only the PMT pins to tightly seal the PMT neck, as illustrated in Fig. 1.

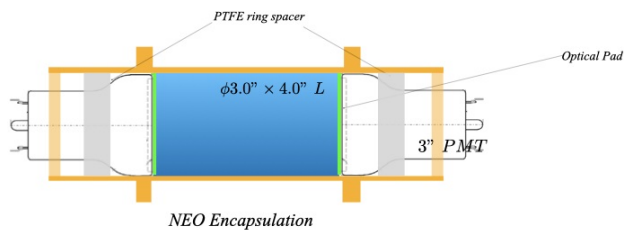


FIG. 1. NaI(Tl) crystal encapsulation design used for the NEON engineering run

For active reduction in radiogenic backgrounds, the NEON detector is installed inside of linear alkylbenzene-based LS [33]. However, this encapsulation design, where the PMT pins and PMT bases are exposed to LS directly, caused the unexpected PMT-induced noise distributed at low energy region. Figure 2(b) visually represents this unexpected noise as an example waveform. It is populated below 10 keV but, broadly distributed upto 50 keV. It is different shape with typical PMT-induced noise due to cherenkov radiation in the PMT glass that generate

fast-decaying noise [34, 36]. Due to its broad range mean-time distribution as shown in Fig. 2(c), these kinds of events are difficult to discriminate from the scintillation events especially at low-energy region below 5 keV.

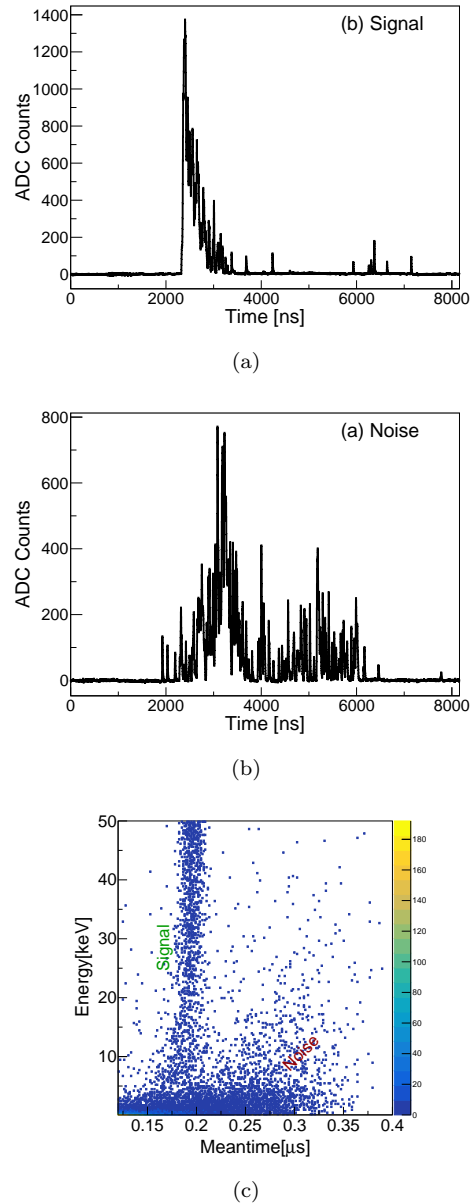


FIG. 2. (a) A waveform of typical scintillation events from NaI(Tl) crystal. (b) An example of the PMT-induced noise events when PMT-base is exposed to LS directly. (c) The mean time distribution with the PMT-induced noise when PMT bases are exposed to LS.

In addition to unexpected PMT-induced noise events, we found that LS can penetrate into the encapsulation in a time scale of a few months. Because of the glass structure of the PMT neck, the pressure to seal the PMT necks was limited. We also found that each PMT had a slightly different geometric shape, making it hard to seal this part perfectly.

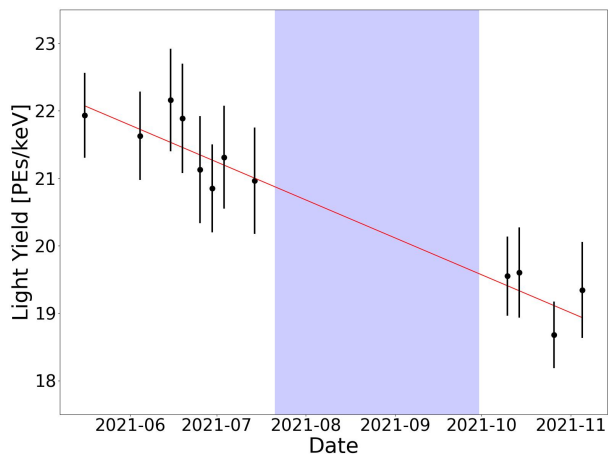
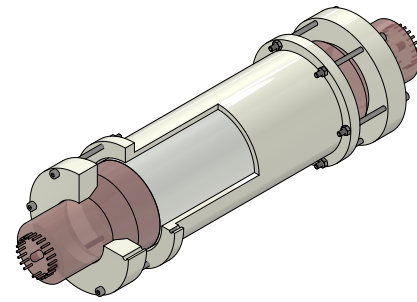


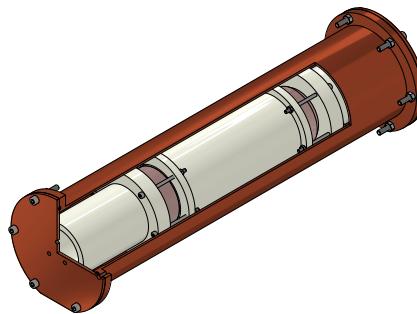
FIG. 3. The DET-4 light yield monitoring while receiving engineering data. The light yield calculation method is described in chapter and didn't take into account low gain of photoelectrons. The colored time periods in the figure represent the time periods during which calibration data was received. During the time of receiving the engineering run, the light yield decreased over time, indicating that the encapsulation design used in the engineering run was not stable enough to maintain light yield.

As a time of a few months in the LS, LS continuously leaked into the encapsulation and defected the crystal surface. Smearing into the optical interface detached the optical coupling as well. All this affected to reduced light yield as a function of time as shown in Fig. 3. Therefore, new encapsulation to protect LS leak into the crystal and the PMT base was necessary.

The new encapsulation comprises two key components: an inner structure dedicated to maintaining a stable coupling between PMT and crystals, and a copper case designed to prevent the infiltration of outside air and LS. A schematic design of the inner structure is shown in Fig. 5(a). The NaI(Tl) crystal is positioned within a polytetrafluoroethylene (PTFE) flanged pipe, enveloped by a soft PTFE film. PMTs are attached to both sides of the crystal using 3-mm thick optical pads. The PTFE flanges are securely fastened to the flanged-pipe by pressing the PMT neck, utilizing six stainless steel bolts on each side. The stainless steel bolts are tightened using a torque wrench to apply same pressure that ensure and maintain optical contact between the PMTs and the crystal. The assembled crystal with PMTs are encapsulated using copper case as one can see in Fig. 5(b). The copper case consists with a flanged pipe shaped encapsulation body and two disk shaped covers. When closing the copper covers, 6 stainless steel bolts in each side are used with a fluorine O-ring. The three cables (anode, dynode signal readouts and high voltage input) in each PMT come out to the outside through waterproof cable glands (AGM6-3) fastened on the cover using fluorine O-ring



(a)



(b)

FIG. 4. Updated design of the NaI(Tl) detector encapsulation. (a) Inner structure for a mounting between the crystal and PMTs. (b) Encasement of the crystal-PMTs structure in the copper case.

and nuts shown in Fig. 5(c). Cable glands are commercial products featuring high waterproofing capabilities, effectively preventing the ingress of LS and external air through the cable exit holes. The crystal detector assembly is shown in Fig. 5.

The entire process of the detector assembly was performed in a glovebox, where the humidity was maintained at less than 10 ppm (H_2O) using Ar gas and a molecular sieve trap. All assembly parts were cleaned to diluted Citranox solution with sonication, baked in a vacuum oven for 12 h, and dried in the glovebox for 2 days before the assembly process.

All detector assembly with the new encapsulation design were completed by March 2022. During upgrade of detector assembly, we replaced two 4-inch length crystals (NEO-1 and NEO-2 [34]) with 8-inch length crystals. NEO-1 and NEO-2 had internal cracks from initial crystal machining resulting reduced light yields and had relatively higher internal backgrounds. The new 8-inch crystals have similar qualities with other 8-inch length crystals, such as NEO-4 and NEO-5 in Ref. [34], in points



FIG. 5. Picture of 4-inch length crystal assembly. (a) Inner structure of 4-inch long crystal and PMTs assembly. (b) Encapsulated detector with copper case and cable grands. (c) Zoomed picture of cable grands to secure detector.

of light output and internal backgrounds. Consequently, a total mass NaI(Tl) crystals were increased from 13.3 kg to 16.7 kg. The crystals relabeled as DET-1 to DET-6 for operational purpose and the physics run started since April 2022.

LIGHT YIELD MEASUREMENT

When measuring light yield, we utilize the 59.54 keV gamma peak from the ^{241}Am source or the internal 46.6 keV gamma plus x-rays or auger electron peak from ^{210}Pb . Light yield is obtained in units of PEs/keV by dividing the total charge at the peak point of the gamma line using corresponding energies with the charge value of the single photoelectron (SPE). To determine the charge value of SPEs, we collect isolated clusters at 2–5 μs from the starting point of the selected gamma line events, minimizing the presence of multiple PE clusters. Although this window reduced the multiple PE clusters, we count up to three SPE merged clusters for the isolated charge distribution modeling.

When a scintillation photon strikes the photocathode of the PMT, it can generate a photoelectron, which undergoes amplification through ten stage dynode structure that typically achieve full amplification, comprising normal gain (NG) processes. Nonetheless, on occasion, a photon may traverse the photocathode and directly strike the first dynode, or a dynode stage may be bypassed due to the back-scattering of the photoelectron at the initial stage of dynode, leading to the production of under-amplified PEs as discussed in Ref. [37]. This phenomenon is referred to as low gain (LG) process.

We developed a fit function to account for both LG characteristics and the presence of multiple PE clusters as described in Ref. [38]. We can obtain the mean charge of NG SPE and a fraction of LG SPE as an example shown in Fig. 6. Typical LG fractions are varied from 5% to 10% similar with Ref. [37].

Due to its relatively low charge of LG SPE events, reconstructions of all LG SPEs from pedestal background are not achievable but approximately an order of 10% of

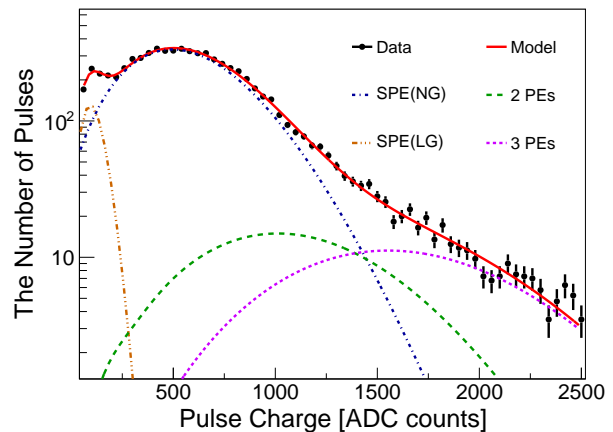


FIG. 6. The charge distribution of the isolated clusters in one PMT of DET-4 is fitted by multiple PE and LG SPE. The SPE mean value resulting from the fitting is 572.8 ADC and the fraction of LG is about 6.8%.

the LG SPEs can be isolated with simple height threshold discrimination depending on PMTs. If we can improve LG SPE reconstruction method from the pedestal, which can be easily improved by accounting shape of the isolated cluster, the effective light yield can be enhanced. In this reason, we account light yields of the NaI(Tl) crystals for both without LG SPEs and with LG SPEs as presented in Table I.

The measured light yields of the NaI(Tl) crystals used in the NEON experiment show mostly above 22 PEs/keV although we do not account LG SPEs. If we can reconstruct 100% of LG SPEs, this yield effectively increase to above 23.5 PEs/keV. The maximum light yield is measured with DET-2 as a 25.6 ± 1.1 PEs/keV without LG SPEs and 27.8 ± 1.4 PEs/keV with LG SPEs. The light yields of each crystals are monitored using the internal peaks of ^{210}Pb decay and stable light yields over one year operation are observed as one can see in Fig. 7. This light yield is well above our initial assumption to achieve more than $3\text{-}\sigma$ sensitivity for CE ν NS observation discussed in

Detector	Mass (kg)	size (inch, D×L)	Light yield	Light yield
			w/o LG (PEs/keV)	w/ LG (PEs/keV)
DET-1	1.67	3 × 4	22.0±0.4	25.3±0.6
DET-2	3.34	3 × 8	25.6±1.1	27.8±1.4
DET-3	1.65	3 × 4	21.8±0.5	23.3±0.9
DET-4	3.34	3 × 8	23.7±0.4	25.4±0.7
DET-5	3.35	3 × 8	22.4±0.5	23.6±0.8
DET-6	3.35	3 × 8	25.0±0.5	27.9±0.7

TABLE I. The light yields of the NEON detector were calculated using two methods. The first method involved using the SPE mean, taking into account only NG SPEs. The second method, on the other hand, consider LG SPEs to account light yield.

Ref. [33]

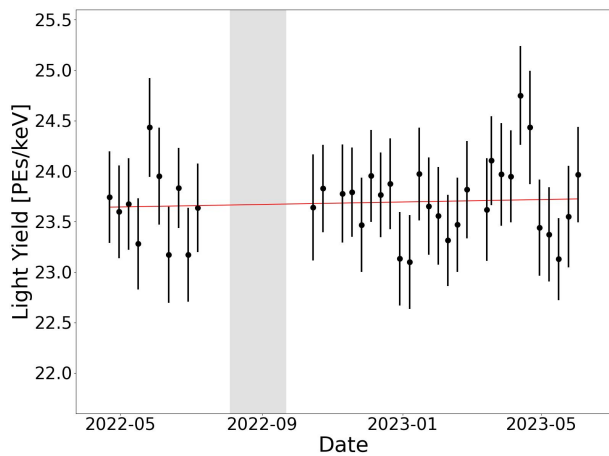


FIG. 7. The DET-4 light yield monitoring while receiving physics data. The colored periods in the figure indicate periods when data collection was interrupted due to power outages and breakdown of high-voltage modules. The light yield of the detectors did not decrease over time during the period of receiving physics data, indicating that the new encapsulation design was stable enough to maintain the light yield.

CONCLUSION

In the article, we introduce a new NaI(Tl) crystal encapsulation for the NEON experiment. High light yield up to 25.6 PEs/keV for a large-size NaI(Tl) crystal with a dimension of 3-inch diameter and 8-inch long cylindrical shape is maintained for approximately one year physics operation. This may allow us to anticipate CE ν NS observation with reactor antineutrinos from the NEON experiment. Similar technique is now applied for the upgrade of the COSINE-100 experiment to enhance light collection efficiency. This encapsulation technique can be applicable for the next generation dark matter

search and CE ν NS experiments using the NaI(Tl) crystals.

ACKNOWLEDGMENTS

We thank the Korea Hydro and Nuclear Power (KHNP) company and particularly acknowledge the help and support provided by the staff members of the Safety and Engineering Support Team of Hanbit Nuclear Power Plant 3. We thank the IBS Research Solution Center (RSC) for providing high performance computing resources. This work is supported by the Institute for Basic Science (IBS) under the project code IBS-R016-A1 and NRF-2021R1A2C1013761.

- [1] D. Z. Freedman, Coherent effects of a weak neutral current, *Phys. Rev. D* 9 (1974) 1389. doi:10.1103/PhysRevD.9.1389. URL <https://link.aps.org/doi/10.1103/PhysRevD.9.1389>
- [2] V. B. Kopeliovich, L. L. Frankfurt, Isotopic and chiral structure of neutral current, *JETP Lett. (USSR) (Engl. Transl.)*, v. 19, no. 4, pp. 145-147 (2 1974). URL <https://www.osti.gov/biblio/4289450>
- [3] A. Drukier, L. Stodolsky, Principles and applications of a neutral-current detector for neutrino physics and astronomy, *Phys. Rev. D* 30 (11) (1984) 2295. doi:10.1103/PhysRevD.30.2295. URL <https://www.scopus.com/inward/record.uri?eid=2-s2.0-33750966650&doi=10.1103%2fPhysRevD.30.2295&partnerID=40&md5=db6a7d821d51b8c47b17be226b568d66>
- [4] L. M. Krauss, Low-energy neutrino detection and precision tests of the standard model, *Phys. Lett. B* 269 (1991) 407. doi:10.1016/0370-2693(91)90192-S.
- [5] K. Patton, et al., Neutrino-nucleus coherent scattering as a probe of neutron density distributions, *Phys. Rev. C* 86 (2012) 024612. arXiv:1207.0693, doi:10.1103/PhysRevC.86.024612.
- [6] B. Dutta, Y. Gao, R. Mahapatra, N. Mirabolfathi, L. E. Strigari, J. W. Walker, Sensitivity to oscillation with a sterile fourth generation neutrino from ultra-low threshold neutrino-nucleus coherent scattering, *Phys. Rev. D* 94 (9) (2016) 093002. arXiv:1511.02834, doi:10.1103/PhysRevD.94.093002.
- [7] T. S. Kosmas, et al., Probing light sterile neutrino signatures at reactor and Spallation Neutron Source neutrino experiments, *Phys. Rev. D* 96 (6) (2017) 063013. arXiv:1703.00054, doi:10.1103/PhysRevD.96.063013.
- [8] P. deNiverville, M. Pospelov, A. Ritz, Light new physics in coherent neutrino-nucleus scattering experiments, *Phys. Rev. D* 92 (9) (2015) 095005. arXiv:1505.07805, doi:10.1103/PhysRevD.92.095005.
- [9] B. Cabrera, L. M. Krauss, F. Wilczek, Bolometric Detection of Neutrinos, *Phys. Rev. Lett.* 55 (1985) 25. doi:10.1103/PhysRevLett.55.25.

- [10] J. A. Formaggio, E. Figueroa-Feliciano, A. J. Anderson, Sterile Neutrinos, Coherent Scattering and Oscillometry Measurements with Low-temperature Bolometers, *Phys. Rev. D* 85 (2012) 013009. [arXiv:1107.3512](#), [doi:10.1103/PhysRevD.85.013009](#).
- [11] D. Yu. Akimov, et al., Prospects for observation of neutrino-nuclear neutral current coherent scattering with two-phase Xenon emission detector, *JINST* 8 (2013) P10023. [arXiv:1212.1938](#), [doi:10.1088/1748-0221/8/10/P10023](#).
- [12] V. Belov, et al., The ν GeN experiment at the Kalinin Nuclear Power Plant, *JINST* 10 (12) (2015) P12011. [doi:10.1088/1748-0221/10/12/P12011](#).
- [13] G. Agnolet, et al., Background Studies for the MINER Coherent Neutrino Scattering Reactor Experiment, *Nucl. Instrum. Meth. A* 853 (2017) 53. [arXiv:1609.02066](#), [doi:10.1016/j.nima.2017.02.024](#).
- [14] A. Aguilar-Arevalo, et al., The CONNIE experiment, *J. Phys. Conf. Ser.* 761 (1) (2016) 012057. [arXiv:1608.01565](#), [doi:10.1088/1742-6596/761/1/012057](#).
- [15] S. Kerman, et al., Coherency in Neutrino-Nucleus Elastic Scattering, *Phys. Rev. D* 93 (11) (2016) 113006. [arXiv:1603.08786](#), [doi:10.1103/PhysRevD.93.113006](#).
- [16] J. Billard, et al., Coherent Neutrino Scattering with Low Temperature Bolometers at Chooz Reactor Complex, *J. Phys. G* 44 (10) (2017) 105101. [arXiv:1612.09035](#), [doi:10.1088/1361-6471/aa83d0](#).
- [17] J. Hakenmüller, et al., Neutron-induced background in the CONUS experiment, *Eur. Phys. J. C* 79 (8) (2019) 699. [arXiv:1903.09269](#), [doi:10.1140/epjc/s10052-019-7160-2](#).
- [18] G. Angloher, et al., Exploring CE ν NS with NUCLEUS at the Chooz nuclear power plant, *Eur. Phys. J. C* 79 (12) (2019) 1018. [arXiv:1905.10258](#), [doi:10.1140/epjc/s10052-019-7454-4](#).
- [19] H. Bonet, et al., Constraints on Elastic Neutrino Nucleus Scattering in the Fully Coherent Regime from the CONUS Experiment, *Phys. Rev. Lett.* 126 (4) (2021) 041804. [arXiv:2011.00210](#), [doi:10.1103/PhysRevLett.126.041804](#).
- [20] D. Akimov, et al., Observation of Coherent Elastic Neutrino-Nucleus Scattering, *Science* 357 (6356) (2017) 1123. [arXiv:1708.01294](#), [doi:10.1126/science.aao0990](#).
- [21] D. Akimov, et al., First Measurement of Coherent Elastic Neutrino-Nucleus Scattering on Argon, *Phys. Rev. Lett.* 126 (1) (2021) 012002. [arXiv:2003.10630](#), [doi:10.1103/PhysRevLett.126.012002](#).
- [22] J. Liao, D. Marfatia, COHERENT constraints on non-standard neutrino interactions, *Phys. Lett. B* 775 (2017) 54. [arXiv:1708.04255](#), [doi:10.1016/j.physletb.2017.10.046](#).
- [23] P. Bhupal Dev, et al., Neutrino Non-Standard Interactions: A Status Report 2 (2019) 001. [arXiv:1907.00991](#), [doi:10.21468/SciPostPhysProc.2.001](#).
- [24] A. Aguilar-Arevalo, et al., Exploring low-energy neutrino physics with the Coherent Neutrino Nucleus Interaction Experiment, *Phys. Rev. D* 100 (9) (2019) 092005. [arXiv:1906.02200](#), [doi:10.1103/PhysRevD.100.092005](#).
- [25] H. T. Janka, Neutrino Emission from Supernovae (2 2017). [arXiv:1702.08713](#), [doi:10.1007/978-3-319-21846-5_4](#).
- [26] B. K. Cogswell, P. Huber, Detection of Breeding Blankets Using Antineutrinos, *Science & Global Security* 24 (2) (2016) 114–130. [doi:10.1080/08929882.2016.1184531](#).
- [27] A. Bernstein, et al., Colloquium: Neutrino detectors as tools for nuclear security, *Rev. Mod. Phys.* 92 (2020) 011003. [doi:10.1103/RevModPhys.92.011003](#). URL <https://link.aps.org/doi/10.1103/RevModPhys.92.011003>
- [28] J. Colaresi, et al., First results from a search for coherent elastic neutrino-nucleus scattering at a reactor site, *Phys. Rev. D* 104 (7) (2021) 072003. [arXiv:2108.02880](#), [doi:10.1103/PhysRevD.104.072003](#).
- [29] Y. J. Ko, et al., Sterile Neutrino Search at the NEOS Experiment, *Phys. Rev. Lett.* 118 (12) (2017) 121802. [arXiv:1610.05134](#), [doi:10.1103/PhysRevLett.118.121802](#).
- [30] G. Adhikari, et al., An experiment to search for dark-matter interactions using sodium iodide detectors, *Nature* 564 (7734) (2018) 83. [doi:10.1038/s41586-018-0739-1](#).
- [31] G. Adhikari, et al., Search for a Dark Matter-Induced Annual Modulation Signal in NaI(Tl) with the COSINE-100 Experiment, *Phys. Rev. Lett.* 123 (3) (2019) 031302. [arXiv:1903.10098](#), [doi:10.1103/PhysRevLett.123.031302](#).
- [32] J. J. Choi, et al., Improving the light collection using a new NaI(Tl) crystal encapsulation, *Nucl. Instrum. Meth. A* 981 (2020) 164556. [doi:https://doi.org/10.1016/j.nima.2020.164556](#).
- [33] J. J. Choi, et al., Exploring coherent elastic neutrino-nucleus scattering using reactor electron antineutrinos in the neon experiment, *Eur. Phys. J. C* 83 (3) (Mar. 2023). [doi:10.1140/epjc/s10052-023-11352-x](#). URL <http://dx.doi.org/10.1140/epjc/s10052-023-11352-x>
- [34] G. Adhikari, et al., Initial Performance of the COSINE-100 Experiment, *Eur. Phys. J. C* 78 (2) (2018) 107. [doi:10.1140/epjc/s10052-018-5590-x](#).
- [35] G. Adhikari, et al., The COSINE-100 liquid scintillator veto system, *Nucl. Instrum. Meth. A* 1006 (2021) 165431. [arXiv:2004.03463](#), [doi:10.1016/j.nima.2021.165431](#).
- [36] K. W. Kim, et al., Tests on NaI(Tl) crystals for WIMP search at the Yangyang Underground Laboratory, *Astropart. Phys.* 62 (2015) 249.
- [37] R. Saldanha, et al., Model independent approach to the single photoelectron calibration of photomultiplier tubes, *Nucl. Instrum. Meth. A* 863 (2017) 35–46. [doi:https://doi.org/10.1016/j.nima.2017.02.086](#). URL <https://www.sciencedirect.com/science/article/pii/S016890021730311X>
- [38] J. J. Choi, et al., Waveform Simulation for Scintillation Characteristics of NaI(Tl) Crystal. (2 2024). [arXiv:2402.17125](#).